J Appl Electrochem (2013) 43:497–505
DOI 10.1007/s10800-013-0532-7

ORIGINAL PAPER

Performance of lithium tetrafluorooxalatophosphate in methyl butyrate electrolytes

Liu Zhou · Mengqing Xu · Brett L. Lucht

Received: 5 November 2012 / Accepted: 24 January 2013 / Published online: 12 February 2013

Abstract Methyl butyrate (MB) has been investigated as a co-solvent for lithium-ion battery electrolytes to improve the performance at low temperature (−10 to −30 °C). The cycling performance of graphite/$LiNi_{1/3}Co_{1/3}Mn_{1/3}O_2$ cells with 1.2 M lithium tetrafluorooxalatophosphate (LiFOP) in 2:2:6 EC/EMC/MB was compared to 1.2 M $LiPF_6$ in both 3:7 EC/EMC and 2:2:6 EC/EMC/MB. The LiFOP/MB electrolyte has a good operational temperature window and comparable cycling performance to the $LiPF_6$ electrolyte at both room temperature and low temperature (−10 °C). However, after accelerated aging the LiFOP/MB electrolyte has worse performance at very low temperature (−30 °C) compared to $LiPF_6$ electrolytes. Ex-situ surface analysis was conducted by scanning electron microscopy, X-ray photoelectron spectroscopy, and Fourier transfer infrared spectroscopy to provide insight into the performance differences.

Keywords Lithium-ion batteries · Electrolytes · Low temperature performance

1 Introduction

Lithium-ion batteries (LIB) have the highest gravimetric and volumetric energy density of commercially produced rechargeable batteries [1]. The incorporation of LIB into portable electronic devices has been occurring for over a decade, but incorporation of LIB into electric vehicles is just beginning. Electric vehicle applications require superior calendar life 10–15 years and a greater operational temperature range, −30 to +60 °C. The electrolyte used in commercial LIB is composed of $LiPF_6$ dissolved in organic carbonates [2]. Ethylene carbonate (EC) is a required component of the electrolyte due to the importance of EC in the formation of the anode solid electrolyte interphase (SEI) [2]. However, the required incorporation of EC leads to poor performance at low temperature due to its high melting point (36.4 °C) [3]. Intensive investigations have been conducted to improve to the performance of lithium-ion cells at low temperature, and a number of electrolyte co-solvents have been identified that can be incorporated into multi-component electrolyte formulations for enhanced performance including ester cosolvents, namely methyl propionate, ethyl propionate, methyl butyrate, ethyl butyrate, propyl butyrate, and butyl butyrate [3–7]. Methyl butyrate (MB) is an excellent co-solvent for improving low temperature performance due to a low melting point (−84 °C) and a low viscosity (0.6 cP) [2].

We have been conducting a detailed analysis of a novel salt, lithium tetrafluorooxalatophosphate [$LiPF_4(C_2O_4)$], which shows many comparable properties with $LiPF_6$, including ionic conductivity, electrochemical stability window, and cycling stability [8–13]. However, $LiPF_4(C_2O_4)$ has better thermal and hydrolytic stability and performance retention upon accelerated aging. While initial investigations of $LiPF_4(C_2O_4)$ with mesocarbon microbead (MCMB) graphite suggested more irreversible capacity during initial formation cycles compared to $LiPF_6$, investigations of natural graphite anodes revealed very similar irreversible capacity during formation cycles for $LiPF_4(C_2O_4)$ and $LiPF_6$ [9]. This unique combination of properties makes $LiPF_4(C_2O_4)$ an interesting alternative to $LiPF_6$.

In this report, the cycling performance of cells with LiFOP/MB electrolyte was investigated with a natural

L. Zhou · M. Xu · B. L. Lucht (✉)
Department of Chemistry, University of Rhode Island, 51 Lower College Road, Kingston, RI 02881, USA
e-mail: blucht@chm.uri.edu

graphite anode and a $LiNi_{1/3}Co_{1/3}Mn_{1/3}O_2$ cathode. Ex-situ surface analysis was conducted by scanning electron microscopy (SEM), X-ray photoelectron spectroscopy (XPS), and Fourier transfer infrared spectroscopy (FT-IR) to understand performance changes after accelerated aging.

2 Experimental

A baseline electrolyte composed of 1.2 M lithium hexafluorophosphate ($LiPF_6$) in 3:7 (vol) ethylene carbonate (EC)/ethylmethyl carbonate (EMC) from Novolyte Corporation was used without further purification (Baseline electrolyte). Lithium tetrafluorooxalatophosphate, $LiPF_4(C_2O_4)$, was synthesized as described previously [6]. $LiPF_6$ (1.2 M) was dissolved in EC/EMC/MB (2:2:6, vol) to generate the $LiPF_6$/MB electrolyte. $LiPF_4(C_2O_4)$ (1.2 M) was dissolved in EC/EMC/MB (2:2:6, vol) to generate the LiFOP/MB electrolyte. Battery grade carbonate solvents, EC and EMC, were obtained from Novolyte Corporation. Methyl butyrate (Acros) was purified by distillation and stored on activated molecular sieves (3 Å) before use.

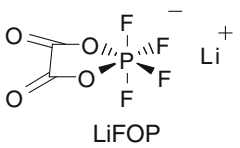

LiFOP

Coin cells (CR2032) were fabricated in a glove box with argon of high purity. The anodes are natural graphite with carboxymethyl starch (CMS) binder and an active material loading of 6.0 mg cm^{-2} was obtained from MTI. The cathode of $LiNi_{1/3}Co_{1/3}Mn_{1/3}O_2$ cells is composed of 92.8 % $LiNi_{1/3}Co_{1/3}Mn_{1/3}O_2$ active material, 4.0 % PVDF, and 3.2 % acetylene black conductive material and was obtained from Lawrence Berkeley National Laboratory (LBNL) and had an active material loading of 13.5 mg cm^{-2}. Between each anode and cathode there is a polypropylene separator which contains 30 μL of electrolyte. The coin cells were cycled with a constant current-constant voltage charge and a constant current discharge between 4.1 and 3.0 V using a battery cycler (BT-2000 Arbin cycler, College Station, TX). The cells were cycled with the following formation procedures: first cycle at C/20, second and third cycle at C/10, and remaining two cycles at C/5. After the initial five formation cycles the cells were cycled at C/5 rate for 5 cycles at room temperature, then 5 cycles at C/10 rate at room temperature charging and low temperature discharging at −10 °C. A Tenny environmental chamber was used to control the temperature (±1 °C). The cells were sealed with epoxy (Torrseal equivalent, Varian) and stored at 55 °C for 1 week to simulate accelerated aging. The stored cells were cycled at C/5 rate for 5 cycles at room temperature again, then 5 cycles at C/10 rate at −10 °C, and 5 cycles at C/10 of room temperature charging and low temperature discharging at −30 °C. Multiple cells of each type were constructed and cycled with good reproducibility. The impedance test was performed on an Ametek PAR VersaSTAT 3 potentiostat with the range of 0.01–10 kHz with a perturbation of 10 mV.

The cells were opened in an Ar glove box after cycling and the electrodes were extracted for surface analysis. The electrodes were rinsed with dimethyl carbonate (DMC) three times prior to surface analysis. The XPS spectra were acquired with a PHI 5500 system using Al Kα radiation (hν = 1,486.6 eV) under ultra high vacuum. Characterization of XPS peaks was made by recording XPS spectra for reference compounds, which would be present on the electrode surfaces: LiF, Li_2CO_3, $Li_xPO_yF_z$, and lithium alkylcarbonate. The graphite peak at 284.3 eV was used as a reference for the final adjustment of the energy scale in the spectra. Lithium was not monitored due to its low inherent sensitivity and small change of binding energy. The spectra obtained were analyzed by Multipak 6.1A software. Scanning electron microscopy images were taken on a JEOL 5900 Scanning Electron Microscope. Fourier transfer infrared spectroscopy (FT-IR) was conducted on a Bruker Tensor 27 Spectrometer with a Pike Miracle attenuated total reflection (ATR) accessory. The spectra were acquired with a resolution of 4 cm^{-1} and a total of 128 scans.

Conductivity measurements were performed with a Thermo Scientific Orion 3 Star conductivity benchtop meter using an Orion 011050MD 2-electrode conductivity probe. The cell constant value is 1.012 cm^{-1}. 10 ml of test electrolyte was put into a threaded Ace glass cell and the cell was sealed with a threaded Teflon adapter and O ring under argon to avoid moisture contamination of the electrolyte. The cell was placed in a Tenney environmental chamber. Conductivity readings were recorded after 3 h equilibration between −30 and 30 °C.

3 Results and discussion

3.1 Cycling performance

Lithium-ion coin cells were constructed containing 1.2 M $LiPF_6$ in 3:7 EC/EMC (baseline electrolyte), 1.2 M $LiPF_6$ in 2:2:6 EC/EMC/MB ($LiPF_6$/MB electrolyte), and 1.2 M LiFOP in 2:2:6 EC/EMC/MB (LiFOP/MB electrolyte) with natural graphite/$LiNi_{1/3}Co_{1/3}Mn_{1/3}O_2$ electrodes. The first cycle efficiencies of the three types of electrolytes were

similar, 87.1, 84.5, and 86.4 %, respectively. After initial formation cycles the cells containing LiFOP/MB electrolyte have a similar cycling performance to the cells containing $LiPF_6$/MB electrolyte, and both of them have better discharge capacity than that of the baseline cells (Fig. 1). When the cells were cooled to −10 °C for low temperature discharging, the discharge capacities of all three sets of coin cells dropped. However, the cells containing methyl butyrate have better discharge capacity (∼120 mAh g^{-1}) than the cells containing baseline electrolyte (∼90 mAh g^{-1}) at −10 °C. The cells were then stored at 55 °C for 1 week to simulate accelerated aging. After aging, the discharge capacities of all sets of coin cells are comparable to the initial room temperature discharge capacities. Upon cycling the cells at low temperature (−10 °C) for a second time, the cells with MB have a slight reduction in discharge capacity compared to the low temperature discharge capacities at −10 °C before aging. The cells containing the baseline electrolyte have very similar discharge capacities at −10 °C before and after aging. Upon lowering the temperature further (−30 °C), all cells have decreased performance, but the cells with LiFOP/MB electrolyte have the lowest discharge capacity (∼35 mAh g^{-1}). The results suggest that while methyl butyrate can improve the low temperature performance of both of $LiPF_6$ and LiFOP electrolyte initially, after accelerating aging cells containing LiFOP/MB electrolyte have poor performance, especially at very low temperatures (−30 °C).

The discharge curves for the cells containing the different electrolytes on the 10th cycle (25 °C) and the 15th cycle (−10 °C) are provided in Fig. 2a. The decrease in the discharge voltage at −10 °C is consistent with increased cell impedance at low temperature for all cells, as expected. The discharge curves for the cells containing different electrolytes after 1 week of storage at 55 °C, cycle 20 (25 °C) and cycle 25 (−10 °C), are provided in Fig. 2b. The discharge curves for the cells cycled at 25 °C are relatively similar before and after storage at 55 °C for 1 week. However, the discharge curve for the cell containing LiFOP/MB electrolyte has a larger decrease in cell voltage than the cells containing the baseline and $LiPF_6$/MB electrolyte. The larger decrease in cell voltage at −10 °C is consistent with an increase in cell impedance after accelerated aging for the cell containing the LiFOP/MB electrolyte.

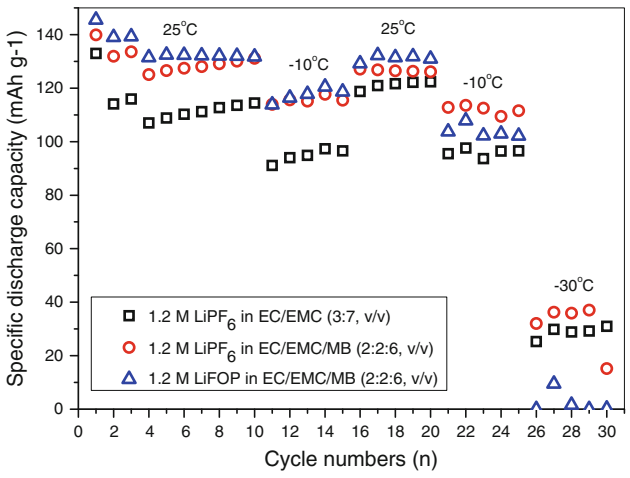

Fig. 1 Cycling performance of 1.2 M $LiPF_6$ in 3:7 EC/EMC, 1.2 M $LiPF_6$ in 2:2:6 EC/EMC/MB, and 1.2 M LiFOP in 2:2:6 EC/EMC/MB in natural graphite/$LiNi_{1/3}Co_{1/3}Mn_{1/3}O_2$ cells

3.2 Electrochemical impedance spectroscopy

The electrochemical Impedance spectra of natural graphite/$LiNi_{1/3}Co_{1/3}Mn_{1/3}O_2$ cells containing baseline electrolyte, $LiPF_6$/MB electrolyte, and LiFOP/MB electrolyte after accelerating aging experiments are provided in Fig. 3. The spectra contain two main features: a higher frequency

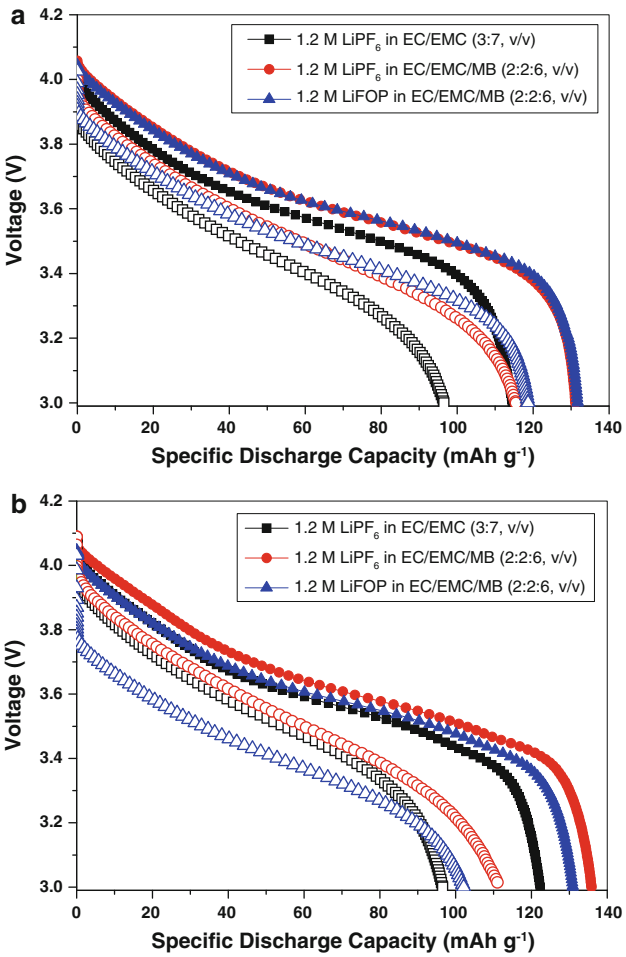

Fig. 2 Discharge Curves of 1.2 M $LiPF_6$ in 3:7 EC/EMC, 1.2 M $LiPF_6$ in 2:2:6 EC/EMC/MB, and 1.2 M LiFOP in 2:2:6 EC/EMC/MB in natural graphite/$LiNi_{1/3}Co_{1/3}Mn_{1/3}O_2$ cells at 25 °C (*solid*) and at −10 °C (*hollow*) **a** before aging; **b** after aging

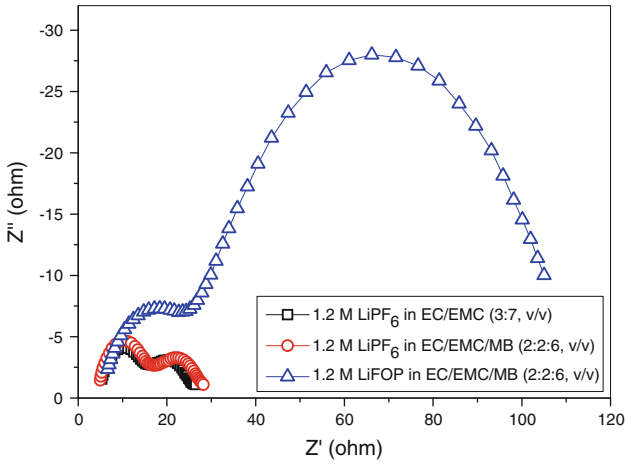

Fig. 3 Electrochemical impedance spectra of natural graphite/$LiNi_{1/3}Co_{1/3}Mn_{1/3}O_2$ cells with 1.2 M $LiPF_6$ in 3:7 EC/EMC, 1.2 M $LiPF_6$ in 2:2:6 EC/EMC/MB, or 1.2 M LiFOP in 2:2:6 EC/EMC/MB after accelerated aging

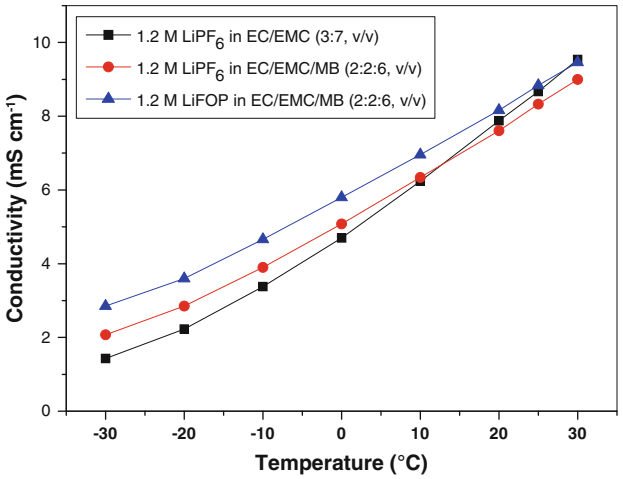

Fig. 4 Ionic conductivity of electrolytes of 1.2 M $LiPF_6$ in 3:7 EC/EMC (vol%); 1.2 M $LiPF_6$ in 2:2:6 EC/EMC/MB (vol%); and 1.2 M LiFOP in 2:2:6 EC/EMC/MB (vol%) between +30 and −30 °C

semicircle, which can be attributed to the impedance response of the surface film formed on the surface of the electrodes and a low frequency semicircle, which can be attributed to charge-transfer processes [14]. The results suggest that the cell with $LiPF_6$/MB electrolyte has similar impedance to the cell with baseline electrolyte; however, the impedance of the cell with LiFOP/MB electrolyte is much greater.

3.3 Ionic conductivity

Ionic conductivity of the baseline electrolyte, the $LiPF_6$/MB electrolyte, and LiFOP electrolyte were measured over the temperature range +30 and −30 °C (Fig. 4). The room temperature ionic conductivity is very similar for all of the electrolytes investigated. However, the addition of MB increases the low temperature ionic conductivity. The LiFOP/MB electrolyte has a higher ionic conductivity than both the baseline electrolyte and the $LiPF_6$/MB electrolyte suggesting that the observed impedance increases may be due to differences in the interphases as discussed below. The LiFOP/MB electrolyte retains good solubility down to −30 °C.

3.4 SEM images

The SEM images of natural graphite anode fresh and after accelerated aging with different electrolytes are depicted in Fig. 5. The surface of the anode materials after aging with either baseline electrolyte or the $LiPF_6$/MB electrolyte contains a thin amorphous coating, which is consistent with the presence of an SEI film. The surface of the anode cycled with LiFOP/MB electrolyte has a much thicker film consistent with a thicker anode SEI.

The SEM images of the $LiNi_{1/3}Co_{1/3}Mn_{1/3}O_2$ cathode fresh and after accelerated aging with different electrolytes are provided in Fig. 6. There are no apparent changes on the cathodes with either electrolyte.

3.5 XPS analysis

The XPS element spectra of natural graphite anodes fresh and after accelerated aging with different electrolytes are provided in Fig. 7 and the elemental concentrations are summarized in Table 1. The composition of the anode is 80.5 % C and 19.5 % O due to the presence of the CMS binder. The C1s spectrum is dominated by the peak characteristic of graphite at 284.3 eV. The peak at 532.5 eV in O1s spectrum is the characteristic peak of the CMS binder. There are no peaks observed in the F1s or P2p spectra.

The surface of the anode after accelerated aging with baseline electrolyte is altered and consistent with previously reported results [14]. The concentration of C is decreased, while the concentrations of F, O, and P are increased. Peaks characteristic of lithium carbonates and alkylcarbonates can be observed in the C1s spectrum at ~290 and 286.5 eV and in the O1s spectrum at 531.6 and 533.5 eV. The F1s spectrum contains a peak characteristic of LiF at 685.0 eV. Evidence of $Li_xPO_yF_z$ is also observed at ~687 eV in F1s spectrum and ~134 eV in P2p spectrum.

Ex-situ surface analysis of the anodes extracted from cells containing $LiPF_6$/MB electrolyte indicates that the concentration of carbon is similar to that of the baseline electrolyte, with a reduced concentration of O and increased concentration of F. The intensity of the C1s peak characteristic of lithium alkylcarbonates (290 eV) has lower intensity while the LiF peak (685.0 eV) in the F1s

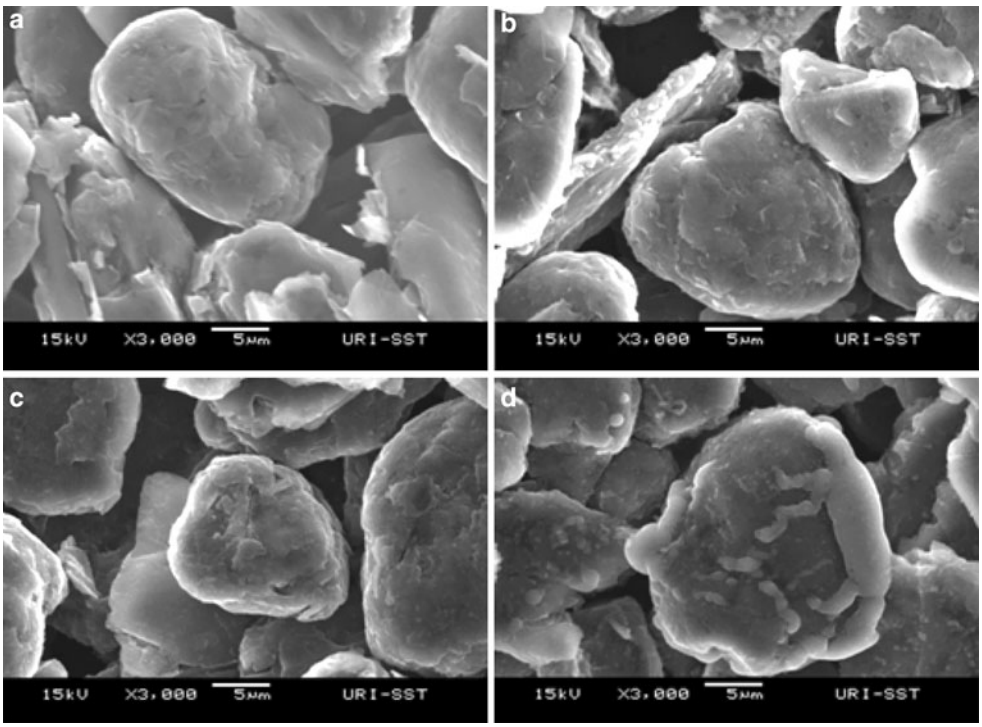

Fig. 5 SEM images of natural graphite anode cycled with $LiNi_{1/3}Co_{1/3}Mn_{1/3}O_2$ cathode **a** fresh; **b** aged with 1.2 M $LiPF_6$ in 3:7 EC/EMC; **c** aged with 1.2 M $LiPF_6$ in 2:2:6 EC/EMC/MB; **d** aged with 1.2 M LiFOP in 2:2:6 EC/EMC/MB

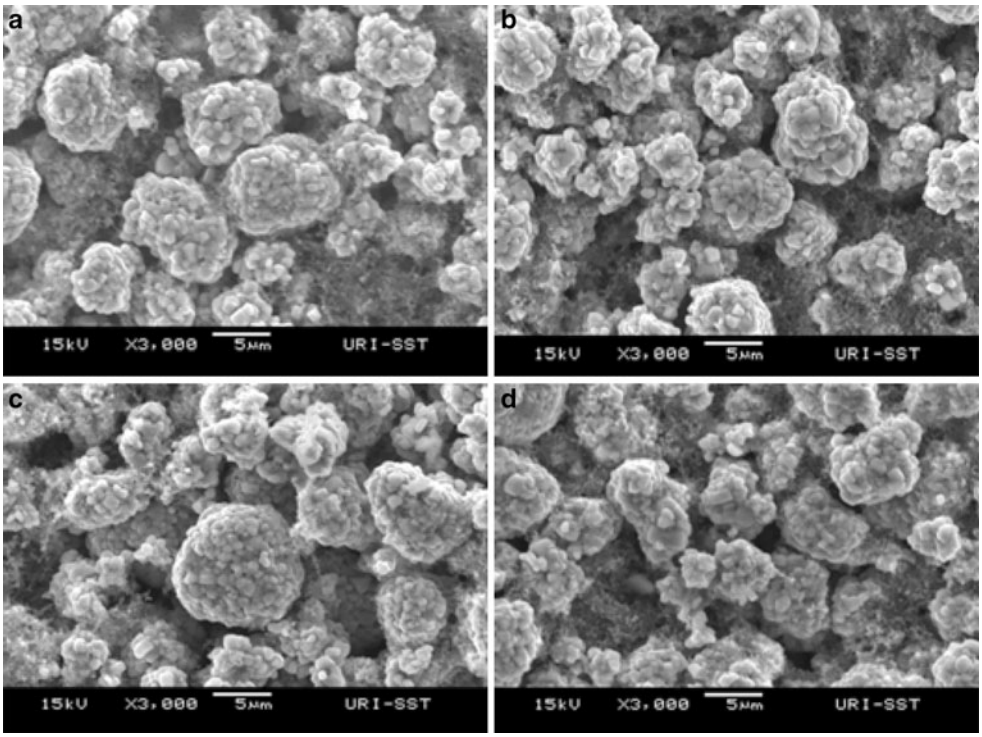

Fig. 6 SEM images of $LiNi_{1/3}Co_{1/3}Mn_{1/3}O_2$ cathode **a** fresh; **b** aged with 1.2 M $LiPF_6$ in 3:7 EC/EMC; **c** aged with 1.2 M $LiPF_6$ in 2:2:6 EC/EMC/MB; **d** aged with 1.2 M LiFOP in 2:2:6 EC/EMC/MB

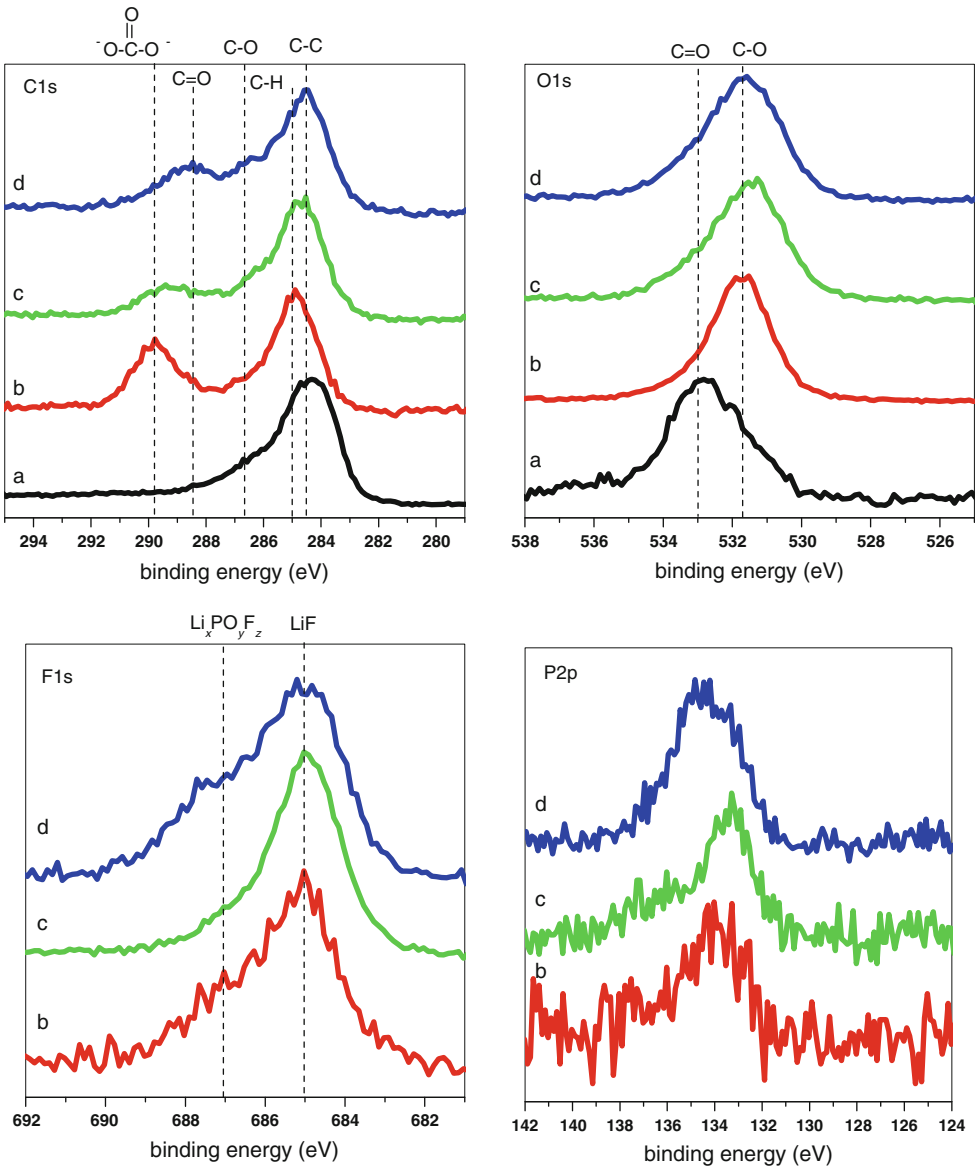

Fig. 7 XPS spectra of natural graphite anode cycled with $LiNi_{1/3}Co_{1/3}Mn_{1/3}O_2$ cathode **a** fresh; **b** aged with 1.2 M $LiPF_6$ in 3:7 EC/EMC; **c** aged with 1.2 M $LiPF_6$ in 2:2:6 EC/EMC/MB; **d** aged with 1.2 M LiFOP in 2:2:6 EC/EMC/MB

Table 1 Elemental analysis of natural graphite anode cycled with $LiNi_{1/3}Co_{1/3}Mn_{1/3}O_2$ cathode

	C1s (%)	O1s (%)	F1s (%)	P2p (%)
Fresh NG	80.5	19.5		
1.2 M $LiPF_6$ in 3:7 EC/EMC	37.3	51.1	10.2	1.4
1.2 M $LiPF_6$ in 2:2:6 EC/EMC/MB	35.4	32.8	29.8	2.0
1.2 M LiFOP in 2:2:6 EC/EMC/MB	55.8	24.5	17.5	2.2

spectrum has increased intensity. The anode of cells aged with LiFOP/MB electrolyte shows a different behavior. The peak characteristic of lithium oxalate is observed at ~288 eV, and more $Li_xPO_yF_z$ is present in the F1s spectrum (~687 eV).

The XPS element spectra of $LiNi_{1/3}Co_{1/3}Mn_{1/3}O_2$ cathodes fresh and extracted from cells cycled with different electrolytes are provided in Fig. 8 and the elemental concentrations are summarized in Table 2. The C1s spectrum of fresh $LiNi_{1/3}Co_{1/3}Mn_{1/3}O_2$ contains three peaks, a peak for graphite at 284.3 eV and peaks for PVdF at 285.7 and 290.4 eV. The peak characteristic of PVdF is also observed in the F1s spectrum at 687.6 eV. The O1s spectrum contains a peak at 529.4 eV characteristic of metal oxide (M–O) and a peak at 531.6 eV from residual Li_2CO_3 on the cathode surface. Ex-situ analysis of the cathode

extracted from a cell cycled with baseline electrolyte suggests that the element concentrations are very similar but small changes are observed in the element spectra. The C1s spectrum is similar to the fresh cathode. A new peak is observed in the F1s spectrum at 684.5 eV, supporting the formation of LiF on the surface of the cathode. The intensity of the O1s peak characteristic of M–O is weaker, while new peaks characteristic of C–O and C=O (533 and 532 eV, respectively) are observed consistent with the deposition of electrolyte decomposition products. A weak peak characteristic of $Li_xPF_yO_z$ is also observed in the P2p spectrum at $\sim$134 eV.

The elemental concentration of the extracted $LiNi_{1/3}Co_{1/3}Mn_{1/3}O_2$ cathode after accelerated aging with $LiPF_6$/MB electrolyte is similar with that of the $LiNi_{1/3}Co_{1/3}Mn_{1/3}O_2$ cathode after aging with baseline electrolyte except that there is a lower concentration of F and a higher concentration of P present on the surface of the cathode aged with $LiPF_6$/MB electrolyte. The peak characteristic of M–O in O1s spectrum of the $LiNi_{1/3}Co_{1/3}Mn_{1/3}O_2$ cathode aged with $LiPF_6$/MB electrolyte has weaker intensity than the $LiNi_{1/3}Co_{1/3}Mn_{1/3}O_2$ cathode aged with baseline electrolyte suggesting the presence of a thicker surface film.

More significant changes in the concentrations of C and F are observed on the surface of the $LiNi_{1/3}Co_{1/3}Mn_{1/3}O_2$ cathodes after aging with LiFOP/MB electrolyte. The concentration of C is decreased significantly while the concentration of F is increased significantly. The peak characteristic of M–O in O1s spectrum is very weak for the $LiNi_{1/3}Co_{1/3}Mn_{1/3}O_2$ cathode after accelerated aging with $LiPF_6$/MB electrolyte suggesting the generation of a thick coating on the surface of the cathode. The peaks

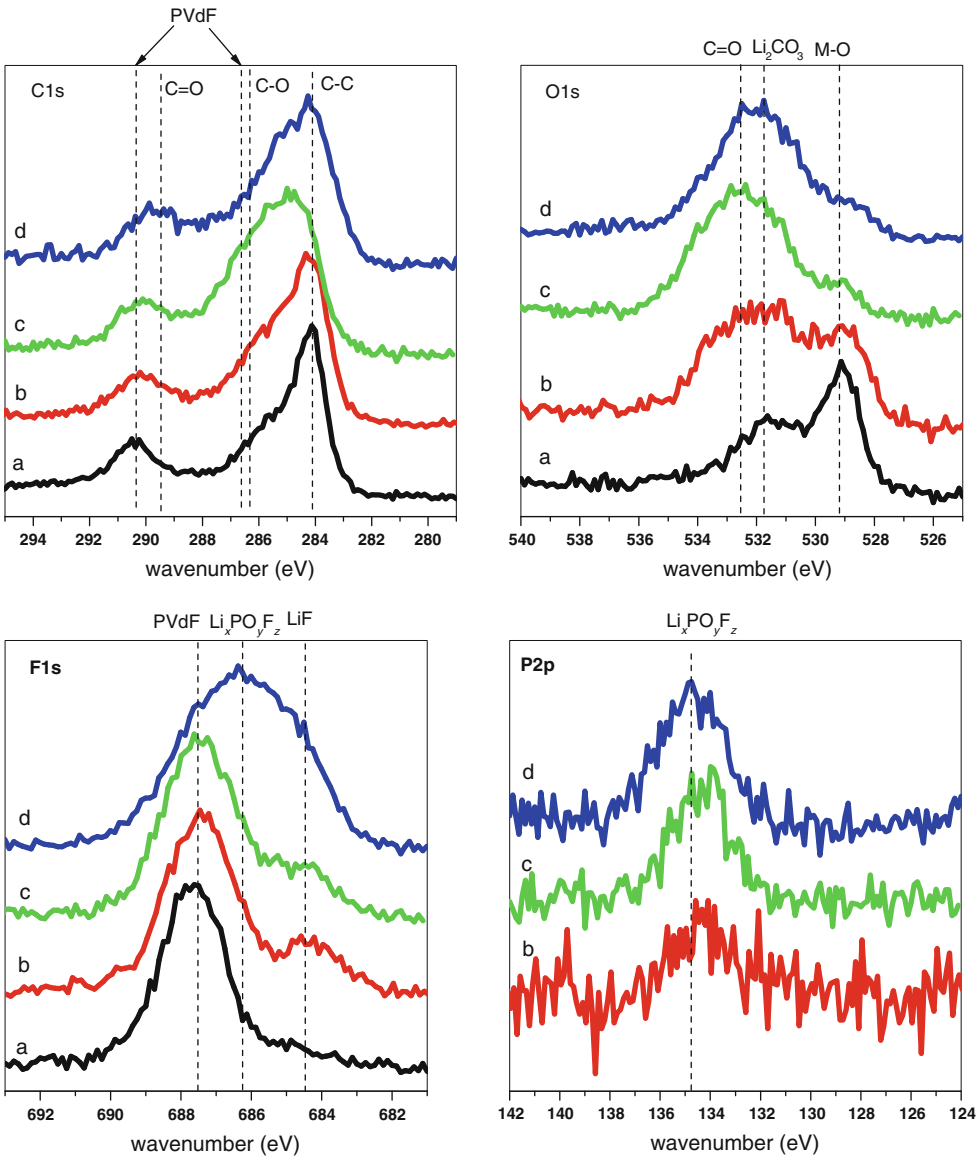

Fig. 8 XPS spectra $LiNi_{1/3}Co_{1/3}Mn_{1/3}O_2$ cathode cycled with a natural graphite anode **a** fresh; **b** aged with 1.2 M $LiPF_6$ in 3:7 EC/EMC; **c** aged with 1.2 M $LiPF_6$ in 2:2:6 EC/EMC/MB; **d** aged with 1.2 M LiFOP in 2:2:6 EC/EMC/MB

Table 2 Elemental analysis of $LiNi_{1/3}Co_{1/3}Mn_{1/3}O_2$ cathode cycled with a graphite anode

	C1s (%)	O1s (%)	F1s (%)	P2p (%)
Fresh NCM	58.2	19.7	22.1	
1.2 M $LiPF_6$ in 3:7 EC/EMC	56.0	20.3	23.2	0.5
1.2 M $LiPF_6$ in 2:2:6 EC/EMC/MB	58.4	21.7	17.2	2.7
1.2 M LiFOP in 2:2:6 EC/EMC/MB	34.6	23.1	37.8	4.5

characteristic of C–O and C=O containing species including lithium alkyl carbonates and oxalates are observed at 286.5 and 289.5 eV in C1s spectrum and 533.5 and 531.5 eV in O1s spectrum, respectively. A small amount of $Li_xPO_yF_z$ is observed in the F1s and P2p spectra at ~587 and ~134 eV, respectively.

3.6 FT-IR spectroscopy

FT-IR spectra of a natural graphite anode fresh and after accelerated aging with different electrolytes are depicted in Fig. 9. The absorption bands in the spectrum of fresh natural graphite result from the CMS binders. The IR spectrum of the natural graphite anode after accelerated aging with the baseline electrolyte contains a peak at 1,427 cm^{-1} characteristic of lithium carbonate, and a small peak characteristic of lithium fluorophosphates at 1,047 cm^{-1}. The IR spectrum of the anode after accelerated aging with $LiPF_6$/MB electrolyte has several new absorptions including peaks for lithium fluorophosphates and Li_2CO_3 and an additional peak at ~1,600 cm^{-1} consistent with the presence of lithium alkyl carbonates.

The IR spectrum of the natural graphite anode after accelerated aging with LiFOP/MB electrolyte is quite different from that of the natural graphite anode after accelerated aging with $LiPF_6$ electrolytes. The presence of lithium oxalate is supported by peaks at ~1,640 and 1,323 cm^{-1}, and poly(ethylenecarbonate) is supported by a peak at 1,760 cm^{-1}. The peaks characteristic of lithium fluorophosphates are also quite intense. The results are consistent with the XPS data of anodes cycled with LiFOP/MB electrolyte.

Figure 10 contains the FT-IR spectra of $LiNi_{1/3}Co_{1/3}Mn_{1/3}O_2$ cathode fresh and after cycling with a natural graphite anode. The peaks of PVdF binder are observed at 1,400, 1,175, and 879 cm^{-1} on the fresh $LiNi_{1/3}Co_{1/3}Mn_{1/3}O_2$ cathode. The IR spectra of the cathodes after accelerated aging are very similar to the IR spectra of the fresh $LiNi_{1/3}Co_{1/3}Mn_{1/3}O_2$ cathode.

4 Conclusions

The first cycle efficiency and cycling performance at room temperature of cells with methyl butyrate ($LiPF_6$/MB and LiFOP/MB) are similar to the cells with baseline electrolyte ($LiPF_6$ in EC/EMC). The cycling performance of electrolytes containing MB are superior to the baseline

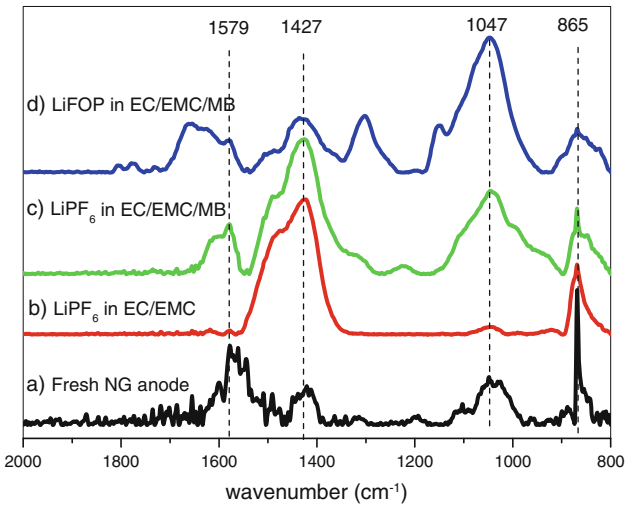

Fig. 9 FT-IR spectra of natural graphite anode cycled with $LiNi_{1/3}Co_{1/3}Mn_{1/3}O_2$ cathode **a** fresh; **b** aged with 1.2 M $LiPF_6$ in 3:7 EC/EMC; **c** aged with 1.2 M $LiPF_6$ in 2:2:6 EC/EMC/MB; **d** aged with 1.2 M LiFOP in 2:2:6 EC/EMC/MB

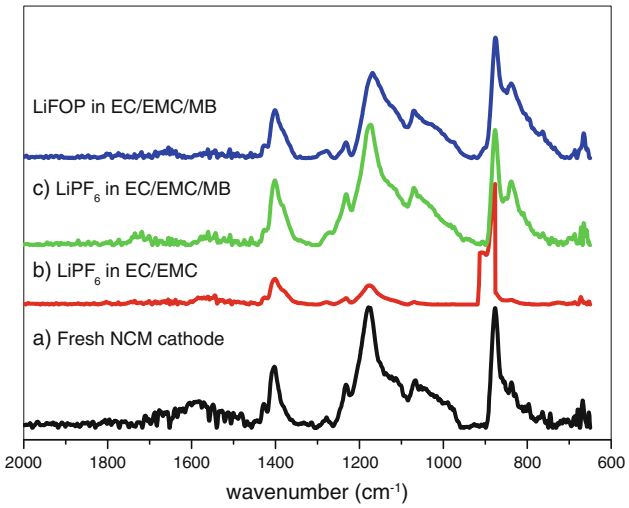

Fig. 10 FT-IR spectra of $LiNi_{1/3}Co_{1/3}Mn_{1/3}O_2$ cathode **a** fresh; **b** aged with 1.2 M $LiPF_6$ in 3:7 EC/EMC; **c** aged with 1.2 M $LiPF_6$ in 2:2:6 EC/EMC/MB; **d** aged with 1.2 M LiFOP in 2:2:6 EC/EMC/MB

electrolyte at low temperature (−10 °C). The LiFOP/MB electrolyte performs well at RT and −10 °C, but does not perform well at −30 °C, especially after accelerated aging experiments. In addition, the LiFOP/MB electrolyte also has better ioninc conductivity at −30 °C than the $LiPF_6$/MB electrolyte or the baseline electrolyte. Finally, the surface analysis suggests that the anode surface film is thicker for cells cycled with LiFOP/MB electrolyte and have high concentrations of lithium oxalate. Thus the data suggest that the poor cycling performance at −30 °C for cells with LiFOP/MB electrolyte is likely due to the thicker surface films on the anode.

Acknowledgments This work was supported by the Assistant Secretary for Energy Efficiency and Renewable Energy, Office of Vehicle Technologies of the U.S. Department of Energy under Contract No. DE-AC02-05CH11231, Subcontract No 6879235 under the Batteries for Advanced Transportation Technologies (BATT) Program.

References

1. Armand M, Tarascon JM (2008) Building better batteries. Nature 451:652–657
2. Xu K (2004) Nonaqueous liquid electrolytes for lithium-based rechargeable batteries. Chem Rev 104:4303–4417
3. Smart MC, Ratnakumar BV, Chin KB, Whitcanack LD (2010) Lithium-ion electrolytes containing ester cosolvents for improved low temperature performance. J Electrochem Soc 157:A1361–A1374
4. Smart MC, Ratnakumar BV, Surampudi S, Wang Y, Zhang X, Greenbaum SG, Hightower A, Ahn CC, Fultz B (1999) Irreversible capacities of graphite in low-temperature electrolytes for lithium-ion batteries. J Electrochem Soc 146:3963–3969
5. Smart MC, Ratnakumar BV, Surampudi S (1999) Electrolytes for low-temperature lithium batteries based on ternary mixtures of aliphatic carbonates. J Electrochem Soc 146:486–492
6. Smart MC, Ratnakumar BV, Surampudi S (2002) Use of organic esters as cosolvents in electrolytes for lithium-ion batteries with improved low temperature performance. J Electrochem Soc 149:A361–A370
7. West WC, Smart MC, Brandon EJ, Whitcanack LD, Plett GA (2008) Double-layer capacitor electrolytes using 1,3-dioxolane for low temperature operation. J Electrochem Soc 155:A716–A720
8. Xiao A, Yang L, Lucht BL (2007) Thermal reactions of $LiPF_6$ with added LiBOB electrolyte stabilization and generation of LiF_4OP. Electrochem Solid-State Lett 10:A241–A244
9. Xu MQ, Xiao A, Li WS, Lucht BL (2009) Investigation of lithum tetrafluorooxalatophosphate ($LiPF_4C_2O_4$) as a lithium ion battery electrolyte. Electrochem Solid-State Lett 12:A155–A158
10. Xu MQ, Xiao A, Li WS, Lucht BL (2010) Investigation of lithium tetrafluorooxalatophosphate [$LiPF_4C_2O_4$] as a lithium-ion battery electrolyte for elevated temperature performance. J Electrochem Soc 157:A115–A120
11. Zhou L, Dalavi S, Xu MQ, Lucht BL (2011) Effects of different electrode materials on the performance of lithium tetrafluorooxalatophosphate (LiFOP) electrolyte. J Power Sources 196:8073–8084
12. Xu MQ, Zhou L, Chalasani D, Dalavi S, Lucht BL (2011) Investigation of the solid electrolyte interphase on MCMB and NG electrodes in lithium tetrafluorooxalatophosphate [$LiPF_4C_2O_4$] based electrolyte. J Electrochem Soc 158(2011):A1202–A1206
13. Zhou L, Lucht BL (2012) Performance of lithium tetrafluorooxalatophosphate (LiFOP) electrolyte with propylene carbonate (PC). J Power Sources 205:439–448
14. Kang SH, Abraham DP, Xiao A, Lucht BL (2008) Investigating the solid electrolyte interphase using binder-free graphite electrodes. J Power Sources 175:526–532